Corrosion protection of steel pipelines with metal-polymer composite barrier liners

Matthew M. Ali [1]

Julia C. Magee [1,2]

Peter Y. Hsieh [1†]

[1] **National Energy Technology Laboratory**
Materials Engineering & Manufacturing Directorate
1450 Queen Ave SW
Albany, OR 97321, USA

[2] School for Environment and Sustainability
440 Church St.
Ann Arbor, MI 48109, USA

E-mail: Peter Y. Hsieh peter.hsieh@netl.doe.gov

Julia C. Magee jcmagee@umich.edu

Matthew M. Ali matthew.ali@netl.doe.gov

Intended for submission to
Journal of Natural Gas Science and Engineering

Date of this version: May 26, 2020

---

[2]Present address

† Corresponding author (Phone: 1-541-967-5983)

Abstract

Pipelines are efficient in transporting natural gas over large distances. Wet carbon dioxide present in pipelines can create an environment that is corrosive to steel. Polymer liners made from either polyethylene or polyamide (nylon) are presently used to mitigate internal corrosion in natural gas pipelines. Gas diffuses through all polymers over time, and polymer-only liners lower the steel corrosion rate by reducing the reactive gas flux to the internal surface of a pipeline. Composite liners, which incorporate one or more metallic layers that are impermeable to corrosive gases, offer better protection than polymer-only liners. We measured the methane, water vapor, and carbon dioxide permeability of a multi-layer barrier film and found it to be more effective in resisting gas permeation than polyethylene and nylon-11 films. The composite barrier film was more effective in protecting steel coupons immersed in a mixture of gaseous methane and wet carbon dioxide at 1 and 24 atm compared with polyethylene and polyamide films.

Keywords: composite liner; corrosion; gas permeability; carbon steel; natural gas pipelines

1. Introduction

Natural gas combined cycle (NGCC) power plants are the most efficient fossil fuel power plants in service today and offer a path towards decarbonized electricity generation when coupled with carbon capture and storage technologies [1]. Moreover, since natural gas power plants can be ramped quickly to meet fluctuations in solar and wind power, they play a vital role in a smart electric power grid [2]. While high-pressure pipelines are the most cost-effective means of transporting natural gas across large distances [3], they are costly to build and construction can be embroiled in political controversy [4, 5]. In addition to supplying NGCC power plants today, existing natural gas transmission pipelines may be called upon to transport carbon dioxide and hydrogen in the future due to the cost and difficulty of building new pipelines.

Wet carbon dioxide and hydrogen are known to have deleterious effects on steel: the former can corrode steel [6] and the latter can embrittle steel [7]. One approach to mitigating potential exposure to carbon dioxide and hydrogen in a multi-product gas pipeline scenario is to use liners with gas barrier properties. Presently, polyethylene (PE) or polyamide (PA) liners are used to protect gathering pipelines from internal corrosion in upstream applications [8, 9]; however, the diffusion of carbon dioxide and hydrogen sulfide over time saturates these polymers [10] and can result in steel corrosion when water is also present [11]. The gas barrier property of the polymeric liner may be improved by adding a continuous metallic foil layer that is physically impermeable to gas diffusion. Metal-polymer composite barrier films have been used for decades to mitigate oxygen and moisture diffusion in food packaging [12]. These barrier films are fabricated from aluminum foil and various polymer layers [13]. Aluminum provides excellent resistance to gas permeation [14] and corrosion [15], while the polymer layers provide both structural support and additional chemical resistance.

Permeation of small gas molecules through polymers occurs through a solution-diffusion mechanism, whereby the gas first dissolves in the polymer, diffuses through the membrane, and then desorbs from the polymer [16]. The permeation coefficient is the product of the solubility and diffusion coefficients for any gas-polymer system [17]. The chemical properties of a polymer and its physical microstructure are important variables in determining the solubility and diffusion coefficients of gases in that polymer [18]. Gas permeation through polymer membranes has been measured using a variety of methods, including: change in system mass [19], change in gas pressure [20-22], or by the change in target gas concentration in a carrier gas through cavity ring-down infrared spectroscopy [23], mass spectrometry [24], or thermal conductivity detection [25].

We measured the permeation of methane, water vapor, and carbon dioxide through five commercial polymers and three aluminum-polymer composite barrier films. Protection against sweet corrosion (by carbon dioxide and water vapor) was evaluated for polyethylene (low-density and high-density), polyamide (nylon-11), and multi-layer foil composite barrier films under ambient conditions and pressurized methane to simulate transmission pipeline conditions.

The multi-layer foil composite barrier film was found to have the lowest gas permeability and the lowest carbonic acid corrosion rate for both ambient and pressurized methane tests.

2. Material and methods

2.1 Polymer and composite film sample characterization

We tested low-density polyethylene (LDPE), high-density polyethylene (HDPE), nylon-11, fluorinated ethylene propylene (FEP), polyvinyl fluoride (PVF), multi-layer foil composite (MLFC), metallized oriented polypropylene (MOPP), and metallized polyethylene terephthalate (MPET). All samples were from commercial vendors and were tested as-received.

A Fourier transform infrared spectrometer (Nicolet iS10) with attenuated total reflectance (ATR) diamond sampling cell was used to analyze all polymers used in this study. Percent transmission as a function of wavenumber (cm^{-1}) was recorded by the instrument software (OMNIC, version 9.2.98). Both the interior and exterior of the MLFC, MOPP, and MPET samples were tested. The ATR sampling cell was cleaned with methanol after each run to avoid contamination.

Composite film samples were cross-sectioned and polished using standard metallography methods, where the final polishing step was 0.25-μm colloidal silica suspension in water. Scanning electron microscopy was used to inspect the thickness of the metallic layers. Film thicknesses were measured using a magnetic coating thickness gauge [26], and are consistent with microscopy results.

Differential scanning calorimetry (DSC) was performed on all polymer samples with a TA Instruments Q200 before and after the water permeation measurements. Test samples weighed 3-5 mg and were loaded into a T-zero aluminum pan. After equilibrating at 25 °C, they were heated at 10 °C/min to 300 °C, then immediately cooled at 10 °C/min to -90 °C. The initial heating and cooling cycles were used to erase the thermal history of the sample, as the previous thermal history affects the measured crystallinity. Samples were then heated at 10 °C/min to 300 °C to measure the glass transition (T_g) and melting transition (T_m) of the polymers. The crystallinity of each sample was calculated via Eq. [1]. The crystallinity was evaluated both as-received from the films and again after the permeation experiments.

$$x_c(\%) = \left[\frac{\Delta H_f}{\Delta H_f^0}\right] * 100 \qquad \text{Eq. 1}$$

2.2 Water permeability measurements

The Standard Test Method for Water Vapor Transmission of Organic Coating Films [27], based on the Payne Cup test [19], was implemented using an environmental glove box and commercially procured 10 cm^2 aluminum permeability cups. A modified version of Test method B (wet cup), condition C (0 % relative humidity, 23 °C) was utilized for this test. In the wet cup test, 10 mL deionized water was placed in the permeability cup, and the membrane or foil sample

was sealed in place across the opening of the cup with a rubber gasket and aluminum sealing ring with three screw-on clamps. The mass of the cup was then measured daily on an analytical balance (Mettler-Toledo AG245, 0.01 mg readability and 0.02 mg repeatability). The permeation of water vapor through the membrane is measured as a change in the mass of the system. The test method specifies that the mass measurements should be made over a three-week interval, or until the change in mass over time becomes constant.

Each material tested in this experiment was tested in triplicate. For each sample, permeability cups (Elcometer 5100/1) were filled with 10 mL of DI water using a pipette. 6.35 cm (2 ½") diameter discs were then cut from each material with scissors. The discs were then sealed on top of the permeation cups, making sure to position the interior of the multi-layer foil composite samples, which came from natural gas sampling bags, facing towards the water.

2.3 Methane and carbon dioxide permeability measurements

Methane and carbon dioxide permeation through each material was measured using a gas permeation cell [28] sampled periodically with a gas chromatograph (Inficon 3000 Micro GC) with thermal conductivity detection (Figure 1). Carbon dioxide was measured using an alumina porous layer open tubular capillary column (PLOT-Q, 8 m × 0.32 mm) with a bonded polystyrene-divinylbenzene stationary phase, while methane was measured using both the PLOT-Q column and a molecular sieve column (MolSieve 5A, 10 m × 0.32 mm) concurrently.

High purity helium (99.999 %) was used as the carrier gas. Table 1 summarizes the conditions under which the measurements were made.

Table 1: The experimental conditions under which the gas chromatograph was held.

Condition	Value
Sample Inlet Temperature	50 °C
Injector Temperature	50 °C
Column Temperature	50 °C
Carrier Gas	Helium
Sweep Flow Rate	1 sccm
Injection Time	100 ms
Nominal Sample Diameter	5.40 cm (2 1/8")

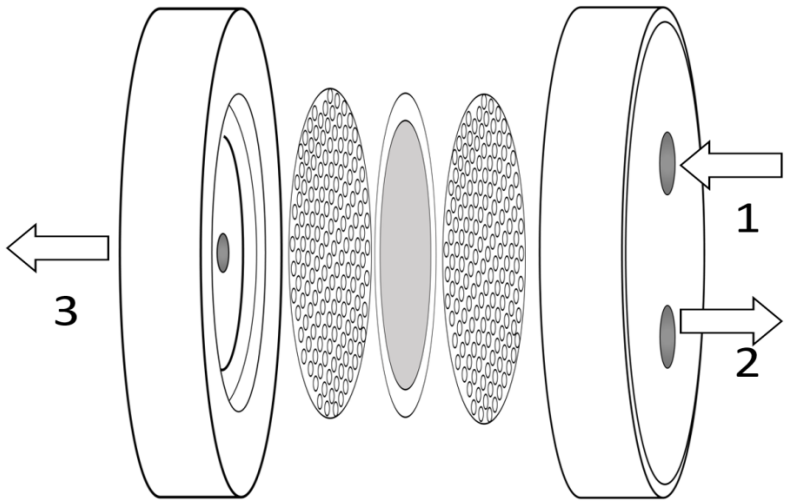

Figure 1: Schematic representation of the permeation cell used to perform the permeation experiments. Flow 1 is the inlet of the process gas with exit as flow 2 and sweep gas, helium as flow 3.

Either methane or carbon dioxide was introduced into the lower compartment of the gas permeation cell at a flow rate of 50 sccm. Helium was used to sweep the gas permeated in the upper compartment of the cell into the gas chromatograph. The gas permeation apparatus was operated at ambient temperature.

2.3.1 Preparation of samples for corrosion measurements

Sample pouches for the ambient and elevated pressure corrosion experiments were prepared with a commercial heat sealer (Impak MP-15). Small swatches of each material (approximately 5 cm × 5 cm) were cut and sealed together with a pressure of 410 kPa (60 psi), heating time of 2 s and cooling time of 4 s. The 1018 steel coupons (1 cm diameter) were weighed on an analytical balance, placed into each pouch, and sealed in the manner shown in Figure 2. Each material tested in this experiment was tested in triplicate.

Figure 2: Steel coupons heat-sealed inside sample pouches. See text for discussion of sealing conditions.

2.4 Ambient pressure water and carbon dioxide corrosion measurements

Ambient pressure immersion experiments were performed with steel coupons which were rinsed with acetone and air dried prior to sealing in sample pouches. Pouches were immersed in 4 L deionized water in a glass reactor with 100 sccm of CO_2 flowing for 65 hours, after which the flow was reduced to 60 sccm for the remainder of the measurements. The ambient temperature was 23 °C with the samples left uninterrupted for 34 days and with the low-density polyethylene samples continuing to 42 days. Each material tested in this experiment was tested in triplicate.

2.5 Elevated pressure water and carbon dioxide corrosion measurements

Elevated pressure immersion experiments were carried out in autoclaves lined with Teflon inserts. 50 mL of deionized water was added to the autoclave and the samples were suspended above the water on a titanium rack horizontally that was encased in Teflon for electrochemical isolation. The autoclaves were sealed, and the head space was displaced via cycle purging with methane. A Haskel model AGD-62 pneumatic high-pressure pump was used to supply gas for experiments and boost pressure to the required experiment conditions. The autoclaves were pressurized with 2300 kPa (22.7 atm) of methane and 210 kPa (2.1 atm) of CO_2 at a rate of 58 kPa/min and held at 25 °C for the duration of the experiment. The 1018 steel coupon samples were exposed uninterrupted for increments of seven days and upon completion of the exposure the autoclaves were depressurized at 690 kPa/min.

3. Results and Discussion

3.1 Polymer and composite material characterization

The thermal analysis of the as-received polymer films and the post-exposure films were analyzed via DSC. The thermogram (Figure 3) shows the results of the heating and cooling cycle on the low-density polyethylene. The glass transition for low-density polyethylene appears at temperatures below what were achievable with the instrumentation. The melting and crystallization peaks appear where expected.

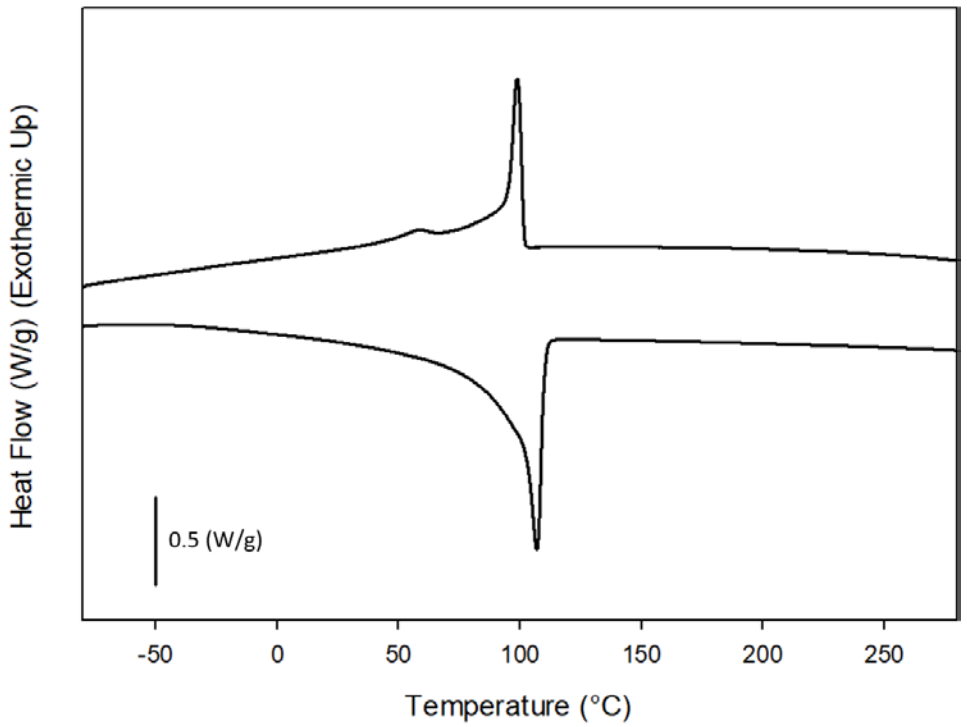

Figure 3: DSC thermogram of low-density polyethylene showing the melting and crystallization peaks. The top curve is exothermic (crystallization) while the bottom curve is endothermic (melting).

Comparing the first heating cycle for the exposed films and the second heating cycle for the as-received films will show the effect of the exposure experiments on the crystallinity of the films as shown in Figure 4 and Table 2. There was no significant change in the crystallinity of either the low-density polyethylene or the nylon-11 films from the elevated pressure exposure experiments. The composite barrier liner contains nylon, polyethylene, and aluminum layers. We assumed that it was unaffected by the effects of experimentation based on the former results.

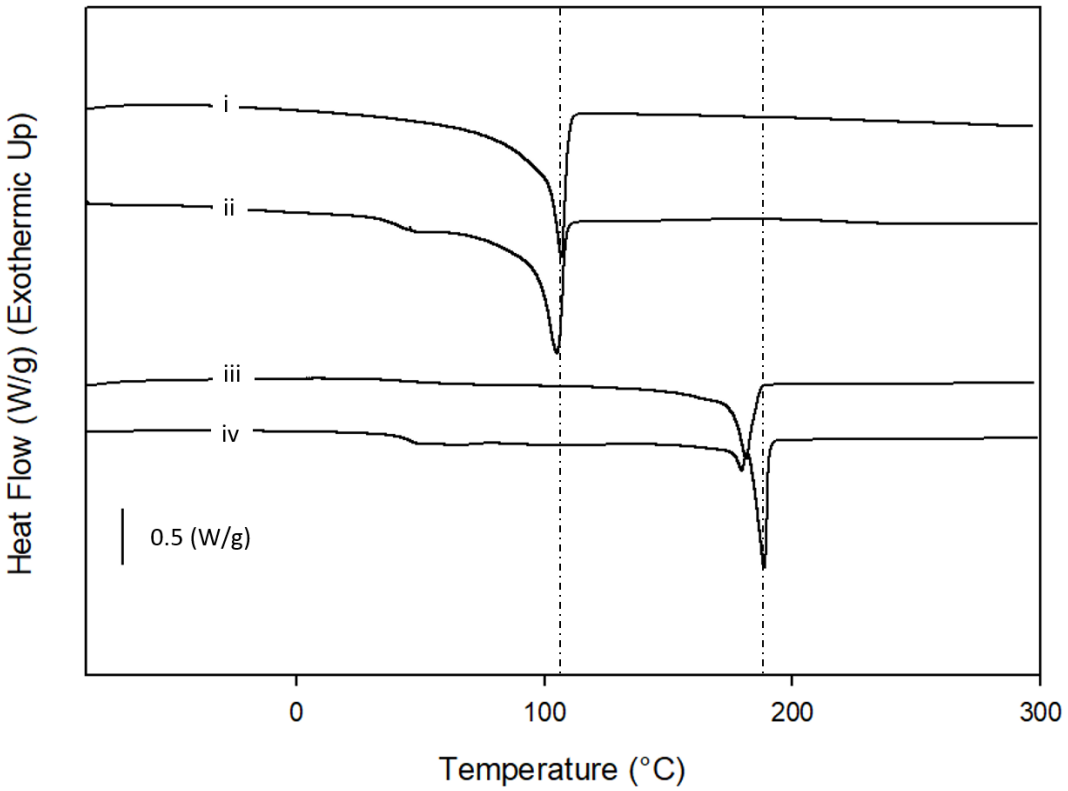

Figure 4: Multiple DSC thermograms showing the melting endotherms for (i) low-density polyethylene film (ii) post-exposure low-density polyethylene film (iii) nylon-11film and (iv) post-exposure nylon-11 film.

Table 2: Tabular data from Figure 2 displaying the melting enthalpy values obtained from differential scanning calorimetry. Asterisks indicate films exposed to gases. Calculating the crystallinity was done using a value of 288.84 (J/g) for low-density polyethylene[29] and 189.05 (J/g) for nylon-11[30].

		1st heat				2nd heat			
	ID	T_g (°C)	T_m (°C)	H_f (J/g)	X_c (%)	T_g (°C)	T_m (°C)	H_f (J/g)	X_c (%)
i	LDPE Film	LL	104.14	140.55	48.66	LL	106.79	138.90	48.09
ii	LDPE Film*	LL	104.69	128.10	44.35	LL	105.58	136.90	47.40
iii	Nylon-11 Film	47.60	188.31	44.06	23.31	40.39	181.44	52.86	27.96
iv	Nylon-11 Film*	46.15	188.62	46.54	24.62	38.39	180.44	54.44	28.80

3.2 Methane, carbon dioxide, and water vapor permeability

Figure 5 is a representative example of data from the gas chromatograph. For the molecular sieve column (i), the single peak at around 40 s corresponds to air (nitrogen and oxygen), while the peak at 42.1 s corresponds to CH_4. For the PLOT-Q column (ii), the CH_4 peak is observed at 74.1 s. The area under each peak is proportional to the amount of the respective gas detected. The methane and carbon dioxide peak areas for each material were numerically integrated (Igor Pro, version

6.37), using Gaussian fits. The average steady-state amount of CH_4 and CO_2 permeation for each material is listed in Table 3.

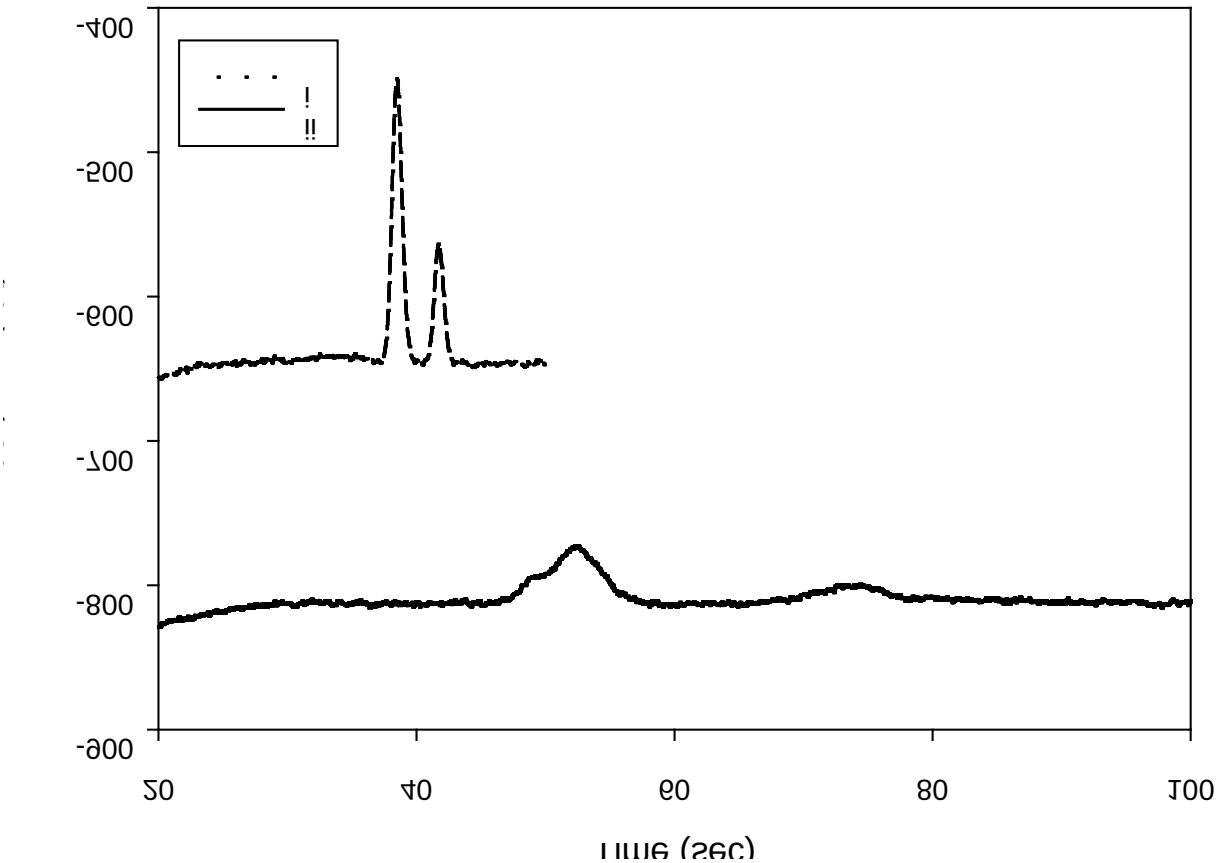

Figure 5. A representative plot of thermal conductivity detector response for molecular sieve (i) and PLOT-Q (ii) columns as a function of time from which the amount of CH_4 permeating through nylon-11 was calculated. See text for discussion of retention times.

MLFC outperforms the single polymer films since its aluminum layer physically blocks the passage of CH_4 and CO_2 through the film. The PVF film also has a relatively low CH_4 and CO_2 permeation value, agreeing with the theory that both polar and nonpolar molecules have low solubility in fluorinated polymers. However, even though FEP is also a fluorinated material, its rates of CH_4 and CO_2 permeation are the third highest among the polymers we tested. Metallized polymers (MOPP and MPET) performed better than polyethylene, but since sputtered aluminum

films are not physically continuous as is the case in a foil, pinhole defects permit a greater rate of gas permeation compared with the MLFC sample.

Table 3. The average amount of CH_4 and CO_2 permeating through each material at steady state. One barrer is equal to 7.5005×10^{-18} $m^2\cdot s^{-1}\cdot Pa^{-1}$ in SI units.

Sample ID	*Corrected CO_2 Permeation* **Barrers**	*Corrected CH_4 Permeation* **Barrers**
High-density polyethylene (HDPE)	34.58 ± 9.07	12.6 ± 1.20
Low-density polyethylene (LDPE)	30.03 ± 6.72	10.15 ± 1.73
Fluorinated ethylene propylene (FEP)	26.07 ± 4.74	4.80 ± 1.16
Metallized Polypropylene (MOPP)	2.19 ± 1.04	0.30 ± 0.10
Nylon-11	1.56 ± 0.32	0.32 ± 0.04
Polyvinyl fluoride (PVF)	0.48 ± 0.07	0.03 ± 0.02
Metallized Polyethylene Terephthalate (MPET)	0.45 ± 0.47	0.49 ± 0.04
Multi-Layer Foil Composite (MLFC)	0.02	--

The water-vapor transmission rate (WVTR) of a film is the quotient of the rate of change of mass (Δm, in g/day) and the area of the film through which water can permeate (A = 0.001 m^2) as shown in equation [2]:

$$P = \frac{|\Delta m|}{A} \qquad (2)$$

The average WVTR values for each material were then calculated, as shown in Table 4. Due to high outdoor temperatures and without the ability to cool the chamber during the experiment, certain data points were collected when the temperature exceeded the ASTM D1653 standard of 25 °C. However, these data points were not included in the determination of the material steady-state slope or the average WVTR.

With the exception of the FEP film, the composite films had lower water-vapor transmission rates than the single polymer films, even though some of the polymer films were thicker than the composites. The aluminum foil layer in MLFC acts as a physical barrier to diffusion and reduces the amount of water-vapor passing through the material. The same concept holds true for the metallized layers in the MOPP and MPET composites. Water, a polar molecule, is expected to be less soluble in a fluorinated material such as FEP. PVF, also a fluorinated polymer, stands out for having a WVTR closer to those of LDPE and HDPE.

Figure 6 summarizes the gas permeation data, with MLFC and MPET being the most promising candidate materials for reducing internal corrosion of steel subject to carbon dioxide and water

exposure in a natural gas pipeline, as it is the most common type of corrosion in oil and gas pipelines [31].

Table 4. The average WVTR values for each material tested, with a reported error of two standard deviations from the mean.

Material	WVTR (g m^{-2} day^{-1})
Nylon-11	17.17 ± 13.11
High-density polyethylene (HDPE)	15.03 ± 5.87
Polyvinyl fluoride (PVF)	13.10 ± 8.38
Low-density polyethylene (LDPE)	11.20 ± 17.60
Metallized Polypropylene (MOPP)	3.67 ± 2.00
Multi-Layer Foil Composite (MLFC)	2.20 ± 4.94
Metallized Polyethylene Terephthalate (MPET)	1.93 ± 2.37
Fluorinated ethylene propylene (FEP)	0.33 ± 0.31

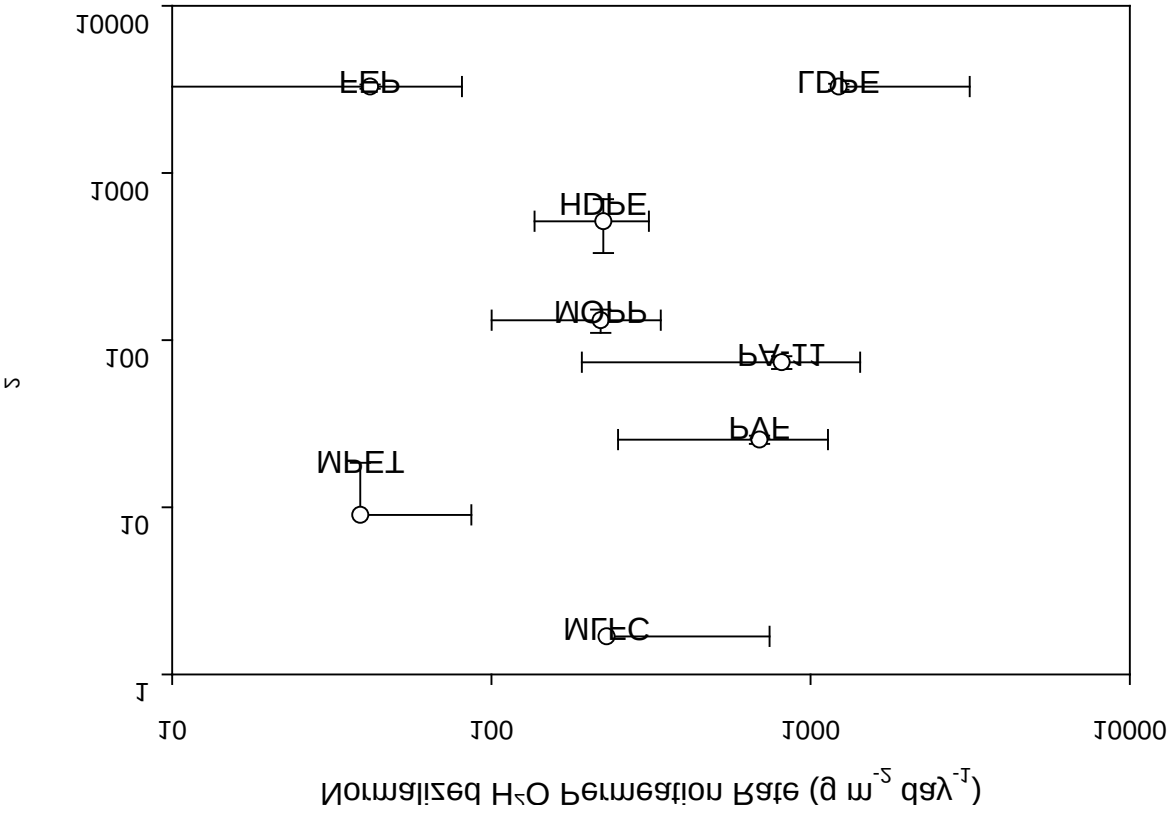

Figure 6. Carbon dioxide and water vapor permeation data of polymer and composite films.

3.3 Ambient pressure sweet corrosion measurements

While dry carbon dioxide does not corrode steel at temperatures typical of oil and gas systems, it can lead to internal corrosion of pipelines when water is also present. The detection of internal corrosion through “smart” pigs with detection and logging tools is a standard industry practice [32]. While corrosion inhibitors are sometimes used to reduce the rate of corrosion [33], this approach may not be technically or operationally feasible. Polymer-metal composite barrier films offer a low-cost alternative to corrosion resistant alloys (stainless steel or nickel-based superalloys).

Polyethylene (PE) or polyamide (PA) liners are used to protect gathering pipelines from internal corrosion in upstream applications [8, 9]. Commercial nylon-11 and LDPE sheets were evaluated against MLFC to determine whether the latter offer greater protection against sweet corrosion as measured by mass change as a function of time.

Figure 7 summarizes the change in steel coupon mass as a function of time for samples enclosed in nylon-11, MLFC, and LDPE pouches immersed in deionized water saturated with carbon dioxide. Since both water and carbon dioxide are necessary to form carbonic acid, coupons enclosed in MLFC should have the smallest amount of carbonic acid exposure. Steel coupons enclosed in the nylon-11 and LDPE pouches were observed to gain mass over time. This is due to the accumulation of corrosion products on the steel surface. Control steel coupons immersed in the same solution were observed to lose mass over time as the corrosion products dissolve in water. Steel coupons enclosed in MLFC had the smallest change in mass, which is consistent with expectations based on gas permeation data.

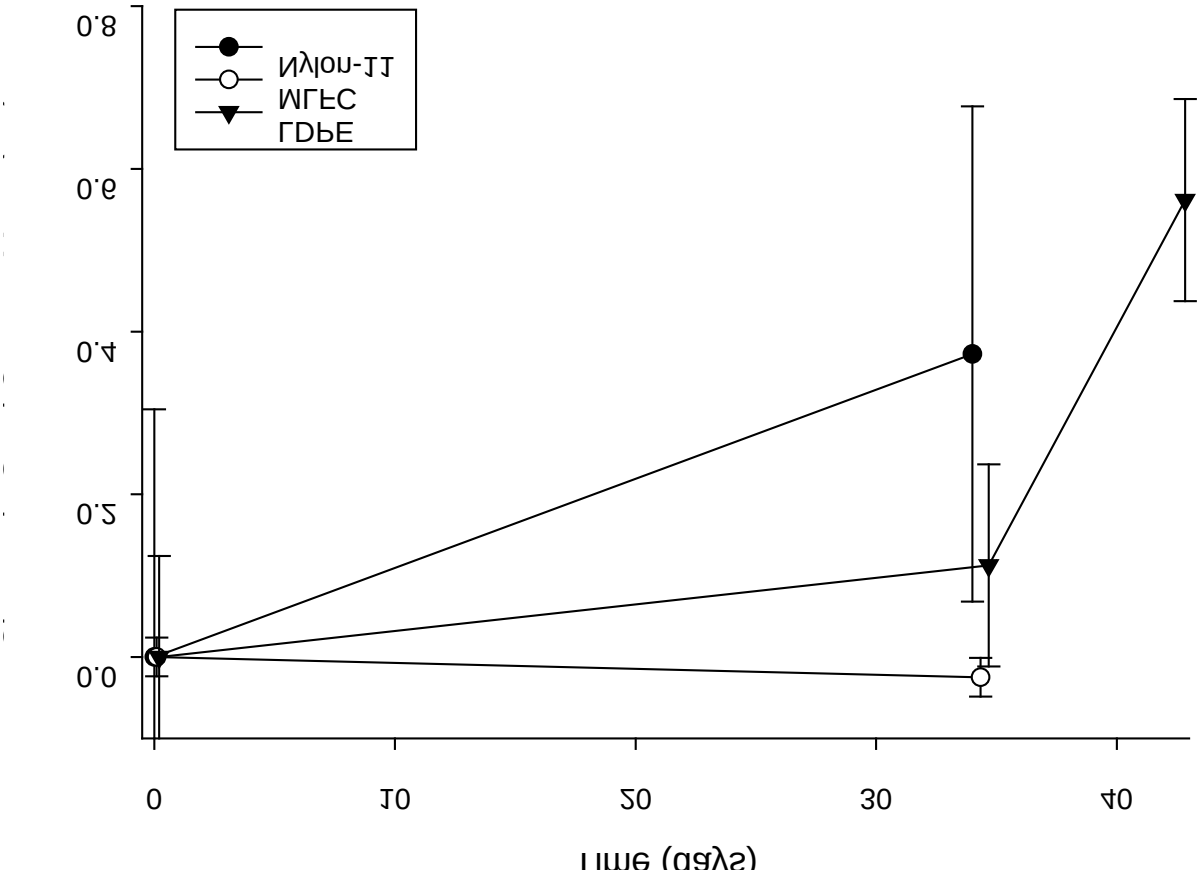

Figure 7: Graph showing the mass change over time of steel coupons enclosed into separate sample pouches at ambient pressure. Error bars reflect standard error with a coverage factor of 2 (95 % confidence interval).

3.4 Elevated pressure sweet corrosion measurements

While gas permeability in polymers typically decreases with pressure, methane and carbon dioxide may have a plasticizing effect on polymers that increases their permeability [34]. The plasticizing effect has been reported for cellulose acetate [35] and poly(methyl methacrylate) [36]. Since natural gas pipelines operate at pressures up to 4 to 94 MPa (3.9 to 93 atm) [37], it is important to repeat the corrosion measurement at higher pressures to ensure that the permeability of the polymers measured under ambient pressures remain relevant at pipeline relevant pressures.

To evaluate the plasticizing effect of methane and carbon dioxide on nylon-11, LDPE, and MLFC and its potential effect on gas permeability, steel coupons were enclosed into individual sample pouches and exposed to wet carbon dioxide and methane gas at elevated pressure. The results are shown in Figure 8.

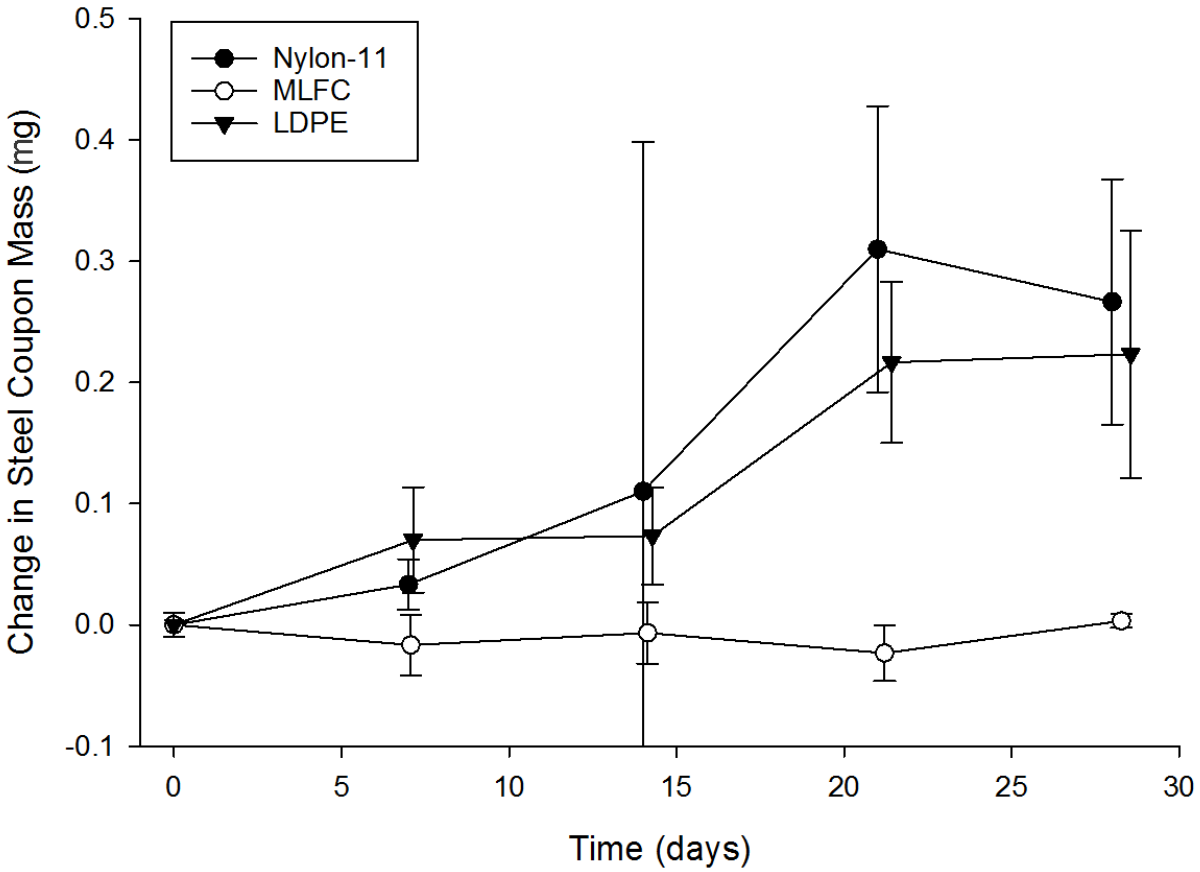

Figure 8: Graph showing the mass change over time of steel coupons enclosed into separate sample pouches at an elevated pressure (34 atm).

The mass gain of the steel coupons protected by the individual pouches is one metric used for assessing the permeation resistance of nylon-11, LDPE, and MLFC. There was a steady mass increase for the steel coupon protected by both the LDPE and nylon-11. There is no discernable mass change of the steel coupons enclosed in the commercial composite pouch. The difference in permeation performance is speculated to be a direct result of the aluminum layers comprising the composite material.

Removal of the steel coupons from sample pouches for weighing likely contributed to the variability in mass change over time. Due to the small size of the samples, it was not possible to re-seal the pouches exactly the same each time a mass measurement was made. The small number of samples tested for each material (n = 3) likely contributes to the scatter in the data.

Images of the sample coupons removed from their protective pouches after the 4-week exposure can be seen in Figure 9. The images confirm that both the coupons enclosed in LDPE and nylon-11 have more corrosion products relative to coupons enclosed in the composite barrier material, which show little to no corrosion. Tests to evaluate the effect of corrosive gaseous environments at either the ambient or elevated pressures on the degradation to the aluminum layers within the composite film are presently underway; however, from visual inspection of the post testing composite barrier films there were no signs of corrosion or discoloration of the aluminum.

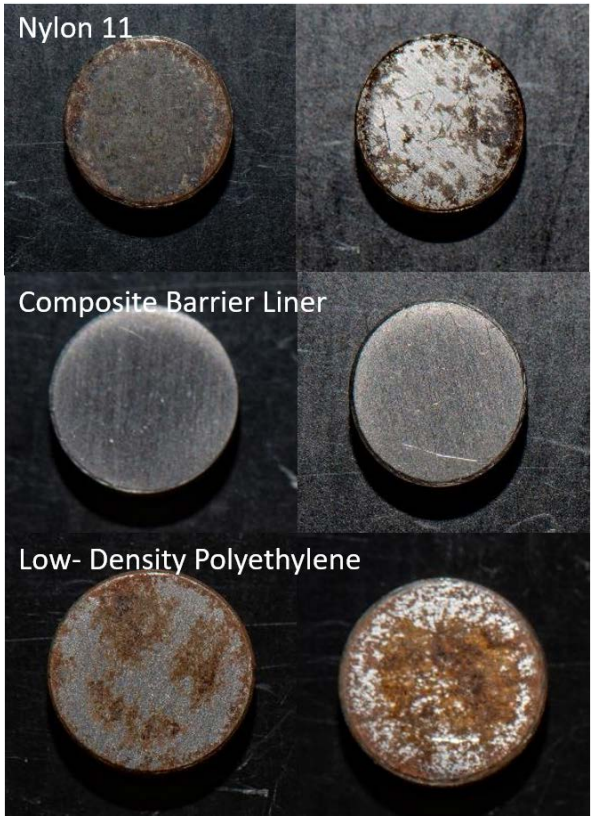

Figure 9: Representative steel coupons removed from their protective pouches after a 4-week long exposure to 34 atm (500 psig) of wet carbon dioxide and methane. The right-hand side is the top of the coupon and left-hand side is the bottom of the coupon.

4. Conclusion

This research demonstrated lower gas permeability through commercial composite films compared with polyethylene and nylon-11. Consistent with the lower measured gas permeability, the composite film is more effective at blocking the diffusion of water and carbon dioxide, which react to form carbonic acid. The composite film is more effective in protecting steel coupons from a wet carbon dioxide corrosive environment at both ambient and elevated pressures. The increased permeation resistance can be attributed to a continuous aluminum layer present in the composite.

This composite structure shows great promise as a method of improving the current pipeline liner technology and protecting the existing pipeline infrastructure, including the possibility for protecting against sweet corrosion for carbon capture and sequestration as well as hydrogen embrittlement with hydrogen-natural gas blends in multi-product pipeline transport scenarios envisioned by the U.S. Department of Energy.

Acknowledgements

This technical effort was performed in support of the National Energy Technology Laboratory's Natural Gas Infrastructure Methane Emissions Mitigation Program. The authors thank Mr. Trevor Godell for machining the steel coupons used in this study, Mr. Jeffrey Oberfoell for laboratory support, as well as Dr. Margaret Ziomek-Moroz for helpful comments on the manuscript. FTIR-ATR measurements were made at Oregon State University. DSC measurements were made at the Center for Advanced Materials Characterization in Oregon (CAMCOR) facility at the University of Oregon.

5. References

[1] N. Khallaghi, D.P. Hanak, V. Manovic, Techno-economic evaluation of near-zero CO_2 emission gas-fired power generation technologies: a review, J Nat Gas Sci Eng, 74 (2020) 13.
[2] J. Jackson, Smart Grids: An Optimised Electric Power System, in: T.M. Letcher (Ed.) Future Energy Elsevier, Boston, 2014, pp. 633-651.
[3] S. Mokhatab, W.A. Poe, J.Y. Mak, Handbook of Natural Gas Transmission and Processing: Principles and Practices, 4th ed., Elsevier Science, 2018.
[4] G.S. Schneider, As court challenges pile up, gas pipeline falls behind, in: Washington Post, Washington DC, 2018.
[5] J. Harper, The unclear future of Nord Stream 2, Russia's controversial gas pipeline, in: Deutsche Welle, 2020.
[6] V.E. Onyebuchi, A. Kolios, D.P. Hanak, C. Biliyok, V. Manovic, A systematic review of key challenges of CO_2 transport via pipelines, Renew Sust Energ Rev, 81 (2018) 2563-2583.
[7] M.W. Melaina, O. Antonia, M. Penev, Blending hydrogen into natural gas pipeline networks: a review of key issues, in, National Renewable Energy Laboratory, Golden, CO, 2013.
[8] D.B. Lebsack, D. Hawn, Internal pipeline rehabilitation using polyamide liners, in: Annual Conference of the National Association of Corrosion Engineers, NACE International, New Orleans, LA, 1997.
[9] G. Siegmund, G. Schmitt, J. Noga, B. Sadlowsky, Lining pipelines with PE - a solution for wet gas transport?, in: Annual Conference of the National Association of Corrosion Engineers, NACE International, Denver, CO, 2002.
[10] F. Sarrasin, P. Memari, M.H. Klopffer, V. Lachet, C. Taravel Condat, B. Rousseau, E. Espuche, Influence of high pressures on CH_4, CO_2 and H_2S solubility in polyethylene: Experimental and molecular simulation approaches for pure gas and gas mixtures. Modelling of the sorption isotherms, J Membrane Sci, 490 (2015) 380-388.

[11] L. Simon, R. MacDonald, K. Goerz, Corrosion failure in a lined sour gas pipeline - part 1: case history of incident, in: NACE Northern Area Western Conference, NACE International, Calgary, Canada, 2010.
[12] A.L. Brody, B. Bugusu, J.H. Han, C.K. Sand, T.H. McHugh, Innovative food packaging solutions, J Food Sci, 73 (2008) R107-R116.
[13] M. Lamberti, F. Escher, Aluminium foil as a food packaging material in comparison with other materials, Food Rev Int, 23 (2007) 407-433.
[14] K. Marsh, B. Bugusu, Food packaging-roles, materials, and environmental issues, J Food Sci, 72 (2007) R39-R55.
[15] B.D. Craig, Handbook of Corrosion Data, ASM International, Metals Park, Ohio, 1995.
[16] P. Tremblay, M.M. Savard, J. Vermette, R. Paquin, Gas permeability, diffusivity and solubility of nitrogen, helium, methane, carbon dioxide and formaldehyde in dense polymeric membranes using a new on-line permeation apparatus, J Membrane Sci, 282 (2006) 245-256.
[17] L.M. Robeson, Correlation of separation factor versus permeability for polymeric membranes, J Membrane Sci, 62 (1991) 165-185.
[18] B. Flaconneche, J. Martin, M.H. Klopffer, Permeability, diffusion and solubility of gases in polyethylene, polyamide 11 and poly(vinylidene fluoride), Oil Gas Sci Technol, 56 (2001) 261-278.
[19] H.F. Payne, W.M.H. Gardner, Permeability of varnish films, Ind Eng Chem, 29 (1937) 893-898.
[20] W. Heilman, V. Tammela, J.A. Meyer, V. Stannett, M. Szwarc, Permeability of polymer films to hydrogen sulfide gas, Ind Eng Chem, 48 (1956) 821-824.
[21] K.C. O'Brien, W.J. Koros, T.A. Barbari, E.S. Sanders, A new technique for the measurement of multicomponent gas transport through polymeric films, J Membrane Sci, 29 (1986) 229-238.
[22] M.A. Del Nobile, G. Mensitieri, A. Sommazzi, Gas and water vapour transport in a polyketone terpolymer, Polymer, 36 (1995) 4943-4950.
[23] P.J. Brewer, B.A. Goody, Y. Kumar, M.J.T. Milton, Accurate measurements of water vapor transmission through high-performance barrier layers, Rev Sci Instrum, 83 (2012) 075118.
[24] B. Flaconneche, J. Martin, M.H. Klopffer, Transport properties of gases in polymers: experimental methods, Oil Gas Sci Technol, 56 (2001) 245-259.
[25] T. Al-Ati, J. Garza, J.H. Hotchkiss, Simple universal permeation apparatus, Packag Technol Sci, 16 (2003) 249-257.
[26] B499-09(2014) Standard Test Method for Measurement of Coating Thicknesses by the Magnetic Method: Nonmagnetic Coatings on Magnetic Basis Metals, in: Annual Book of ASTM Standards, ASTM International, West Conshohocken, PA, 2014.
[27] D1653-13 Standard Test Methods for Water Vapor Transmission of Organic Coating Films, in: Annual Book of ASTM Standards, ASTM International, West Conshohocken, PA, 2013.
[28] H. Lin, E. Van Wagner, B.D. Freeman, L.G. Toy, R.P. Gupta, Plasticization-enhanced hydrogen purification using polymeric membranes, Science, 311 (2006) 639.
[29] P.N. Khanam, M.A.A. AlMaadeed, Processing and characterization of polyethylene-based composites, Advanced Manufacturing: Polymer & Composites Science, 1 (2015) 63-79.
[30] P. Latko, D. Kolbuk, R. Kozera, A. Boczkowska, Microstructural Characterization and Mechanical Properties of PA11 Nanocomposite Fibers, Journal of Materials Engineering and Performance, 25 (2016) 68-75.

[31] M. Askari, M. Aliofkhazraei, S. Afroukhteh, A comprehensive review on internal corrosion and cracking of oil and gas pipelines, J Nat Gas Sci Eng, 71 (2019) 102971.
[32] S.M. Folga, Natural gas pipeline technology overview, in, Argonne National Laboratory, Argonne, IL, 2007.
[33] M. Askari, M. Aliofkhazraei, S. Ghaffari, A. Hajizadeh, Film former corrosion inhibitors for oil and gas pipelines - A technical review, J Nat Gas Sci Eng, 58 (2018) 92-114.
[34] R.T. Chern, C.N. Provan, Gas-induced plasticization and the permselectivity of poly(tetrabromophenolphthalein terephthalate) to a mixture of carbon dioxide and methane, Macromolecules, 24 (1991) 2203-2207.
[35] M.D. Donohue, B.S. Minhas, S.Y. Lee, Permeation behavior of carbon dioxide-methane mixtures in cellulose acetate membranes, J Membrane Sci, 42 (1989) 197-214.
[36] Y.P. Handa, P. Kruus, M. O'Neill, High-pressure calorimetric study of plasticization of poly(methyl methacrylate) by methane, ethylene, and carbon dioxide, J Polym Sci Pol Phys, 34 (1996) 2635-2639.
[37] G.G. Nasr, N.E. Connor, Transmission and Distribution Systems and Design, in: Natural Gas Engineering and Safety Challenges: Downstream Process, Analysis, Utilization and Safety, Springer International Publishing, Cham, 2014, pp. 17-43.